JOURNAL OF AIRCRAFT
Vol. 31, No. 2, March–April 1994

Propulsion-Induced Aerodynamic Effects Measured with a Full-Scale STOVL Model

Brian E. Smith*
NASA Ames Research Center, Moffett Field, California 94035
William A. Poppen†
General Dynamics, Fort Worth, Texas 76101
and
J. David Lye‡
de Havilland Incorporated, Toronto, Ontario, Canada

Propulsion-induced aerodynamic interference effects are presented for a full-scale, powered, STOVL fighter aircraft model. The ejector-lift/vectored thrust configuration, designated the E-7A, was tested at low speed in the 40- by 80- and 80- by 120-ft wind tunnels of the National Full-Scale Aerodynamics Complex located at NASA Ames Research Center. Aerodynamic effects on vehicle lift, drag, and pitching moment are presented over a range of effective velocities for simultaneous operation of all lifting jets. The jet/airframe interactions for separate operation of the lifting ejector system and vectorable ventral nozzle are also presented. Ejector and engine inlet momentum effects were fully simulated in these full-scale, powered tests. The jet thrust vector angle of the ventral nozzle was varied to simulate transition from hover to wingborne flight modes. When the lifting ejector system and ventral nozzle are operated simultaneously, the induced effects on lift decrease as the thrust vector angle of the ventral nozzle approaches the horizontal. A negative increment in drag is produced over a narrow portion of the transition speed range when the ejectors and ventral nozzle are operated together. Aerodynamic induced effects of the ejector system measured at full-scale compare well with the small-scale data. Changes in lift and pitching moment due to ventral nozzle operation are smaller at full scale.

Nomenclature

A = nozzle exit area, in.^{2}
C_D = total drag coefficient
$C_{D,A}$ = thrust removed drag coefficient
C_L = total lift coefficient
$C_{L,A}$ = thrust removed lift coefficient
C_M = total pitching moment coefficient
$C_{M,A}$ = thrust removed pitching moment coefficient
c = chord
D = measured drag
D_{ram} = inlet ram drag, lbf
d_{ej} = moment arm of ejector thrust, ft
d_{ejinl} = moment arm of ejector inlet drag, ft
d_{in} = moment arm of engine inlet drag, ft
d_{rn} = moment arm of rear nozzle thrust, ft
d_{vn} = moment arm of ventral nozzle thrust, ft
L = measured lift
M = measured pitching moment
$\dot{m}$ = mass rate of flow, lbm/s
m.a.c. = mean aerodynamic chord, 282.68-in. full-scale
q_j = dynamic pressure of jet
q_∞ = freestream dynamic pressure, lbf/ft^2
S = reference planform area, 630.6-ft^2 full-scale
T = static thrust, lbf
T_{ej} = ejector thrust, lbf
T_{rn} = rear nozzle thrust, lbf
T_{vn} = ventral nozzle thrust, lbf
V_e = effective jet velocity
V_{e_w} = average weighted effective velocity
V_∞ = freestream velocity
α = angle of attack, deg
ΔD = propulsion-induced drag, lbf
ΔL = propulsion-induced lift, lbf
ΔPM = propulsion-induced pitching moment, ft-lbf
δ_{vn} = ventral nozzle thrust vector angle, deg
μ = mass flow ratio, $\dot{m}_s/\dot{m}_p$

Subscripts
ej = ejector
ejinl = ejector inlet
in = engine inlet
p = primary
rn = rear nozzle
s = secondary
vn = ventral nozzle

Introduction

THE interaction between propulsive, lifting jet exhaust streams and the airframe of a short takeoff/vertical landing (STOVL) aircraft can have a significant influence on the aerodynamic performance of the aircraft in the transition flight regime. The high-energy exhaust jets emanating from the lower surface of the vehicle interact with the freestream flow to create high-energy vortices which roll up under the wing, significantly altering the flowfield on the lower surface.[1] Jet entrainment effects can also significantly change the flowfield in which the wing is immersed.[2] The principal effects of operation of lifting jets are to induce lift losses on the wing and introduce drag and pitching moment increments on the airframe. For satisfactory transition flight characteristics, the sum of jet and wingborne lift in the low-speed range must be sufficient to overcome the induced lift losses. An operational

Presented as Paper 91-0765 at the AIAA 29th Aerospace Sciences Meeting, Reno, NV, Jan. 7–10, 1991; received Jan. 3, 1992; revision received Dec. 10, 1992; accepted for publication Jan. 20, 1993.

*Aerospace Engineer. Senior Member AIAA.
†Senior Engineer.
‡Senior Research Engineer.

STOVL vehicle must also have sufficient thrust vectoring and pitch trim capability to offset the jet-induced changes in drag and pitching moment during transition.

On aircraft equipped with lifting ejectors such as the E-7A STOVL concept, the entrainment of freestream air into the ejector inlets can also have a significant effect on the overall aerodynamic performance of the aircraft. The negative pressures induced on the inlet and adjacent wing surfaces can have large effects on the vehicle pitching moment characteristics. This is especially true for configurations such as the E-7A in which the ejector inlets are located near the apex of the wing planform forward of the c.g. of the aircraft. Local perturbations in the wing pressure distribution can also affect the lift generated by the wing at low speeds. Earlier tests of powered, scale models of the E-7A at NASA Langley and IAR Ottawa predicted significant effects.[2-7] These analyses have attempted to quantify the propulsion-induced aerodynamics in transition for the E-7A concept. Data from the scale model investigations have been used to assess the propulsion-induced aerodynamic interference of lifting ejectors and ventral nozzles when operated separately.

A unique aspect of the present work is that the induced-effects data were acquired using a full-scale, powered model. In powered-lift experimental work, the question of scale effects inevitably arises, particularly with respect to proper simulation of jet exit conditions[1,8] and in the modeling of ejector augmentors.[9] In order to minimize uncertainties in the prediction of flight vehicle performance based on scale-model hover and transition data, a full-scale, jet-engine-powered model of the E-7A configuration was constructed. The model, mounted in the Ames 80- by 120-ft wind tunnel test section, is shown in Fig. 1.

The primary purpose of the present investigation is to examine the jet-induced changes in lift, drag, and pitching moment on a representative full-scale STOVL configuration when multiple lifting jets of significantly different exit velocities are operated simultaneously and with all inlet flows properly simulated. An important characteristic of the E-7A configuration is that although there is approximately an equal thrust split between the ejectors and ventral nozzle, there is a large difference in the velocities of the jet efflux between the two lifting systems. The exit area of the ejectors is more than an order of magnitude greater than the exit area of the ventral nozzle (34.1 ft^2 for the ejectors vs 2.33 ft^2 for the ventral nozzle). This results in dramatically higher jet loading for the ventral nozzle when compared with the ejector system (2830 lb/ft^2 for the ventral nozzle vs 179 lb/ft^2 for the ejectors).

This article summarizes the analysis of the transition aerodynamics data for the E-7A configuration obtained from tests of the model in the facilities of the National Full-Scale Aerodynamics Complex located at NASA Ames Research Center. High-speed transition tests were performed in the 40- by 80-ft test section. Low-speed and hover performance data were obtained in the 80- by 120-ft test section in order to minimize wind-tunnel wall effects. Comparisons of these data with scale-model tests results from NASA, General Dynamics, and de Havilland Incorporated (DHI) are also presented.

Description of Model and Wind Tunnels

The E-7A wind-tunnel model is based on the results of a General Dynamics design study[9,10] which explored various aircraft and propulsion system configurations. The E-7A (Fig. 2) employs a separate flow propulsion system where the engine core flow exhausts from a vectoring ventral nozzle, and the bypass flow exhausts from a rear fuselage nozzle in wing-borne flight or from a set of thrust augmenting ejectors forward of the c.g. for balance in transition and hover. The E-7A model, including the high-performance lifting ejector system, was designed by DHI and built by DHI and NASA Ames personnel.[11,12]

The full-scale model has the same planform as the General Dynamics E-7A design (Fig. 2), but has a different wing airfoil section with a camber and twist distribution chosen by NASA Ames. The airfoil used for the model is a NACA 630004 section, and a 6 deg (leading edge down) linear twist distribution was applied to the wing (with zero twist at the exposed root chord). The twist axis is located along the hinge line of the trailing-edge flaperons. The moment reference center is located at 34% m.a.c.

The model is powered by a Rolls-Royce Spey 801-SF split flow turbofan which has a modified operating line such that the fan is overdriven to provide ejector primary nozzle pressure ratios close to the range of interest. Total available engine thrust is 10,450 lbf with 63% delivered to the ventral nozzle and the remaining 37% delivered to the ejectors/rear nozzle. When the ejectors are deployed for hover, the ejector augmentation ratio of 1.58 increases the primary thrust to a total ejector thrust of 6117 lbf. As a result, the total augmented thrust for the model in hover mode (ejectors operating, δ_{vn} = 90 deg) is 12,700 lbf with a thrust split of 48/52% between the ejector system and ventral nozzle. A large-radius, subsonic inlet is used on the full-scale model in place of the relatively sharp supersonic inlet with blow-in doors used in the original E-7A design since supersonic performance is not required of the model.

Figure 3 shows a three-view diagram of the propulsion system used in the E-7A model. Bypass air from the engine is routed to twin plenums located in the upper fuselage. From these plenums, air can be delivered to the ejector system primary nozzles and/or to the rear nozzle depending on the butterfly throttling valve settings. The core air from the turbofan exhausts through a rectangular ventral nozzle with aspect ratio 3.5. The major axis of the ventral nozzle is oriented

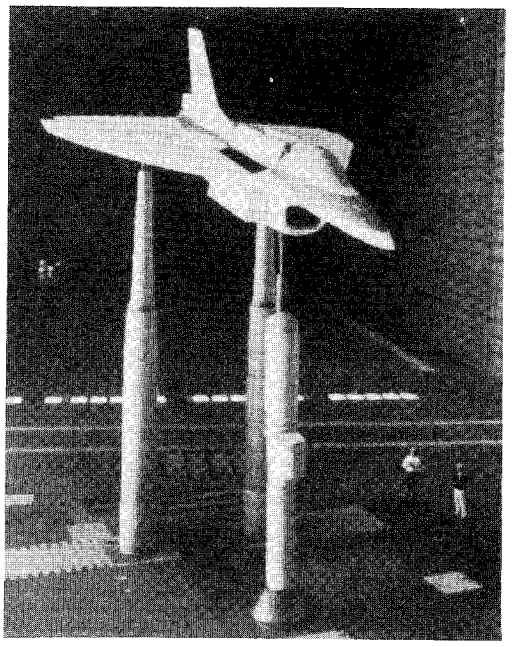

Fig. 1 E-7A Wind-tunnel model in 80- by 120-ft wind tunnel.

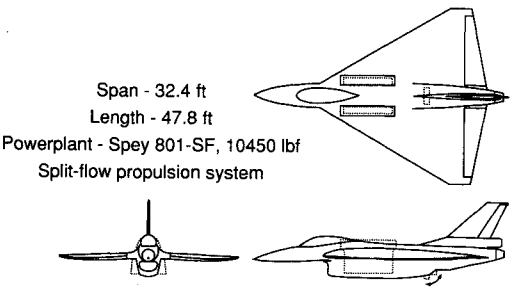

Fig. 2 Three-view sketch of full-scale E-7A model.

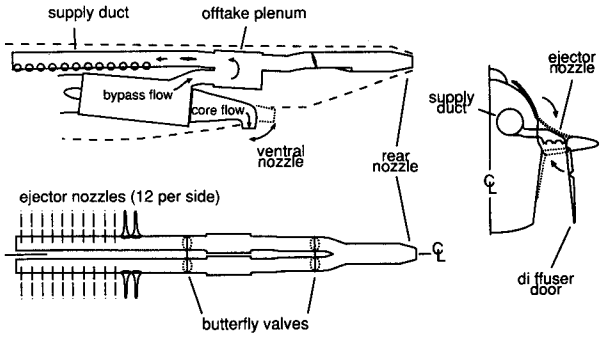

Fig. 3 Ejector system diagram.

transversely. Vectoring of the ventral nozzle is accomplished by interchanging four fixed geometry nozzles with deflection angles of 6, 30, 60, and 90 deg from the horizontal.

The model was tested extensively in the wind-tunnel facilities of the National Full-Scale Aerodynamics Complex located at Ames Research Center. In the fall of 1988, the E-7A occupied the test section of the closed-return 40- by 80-ft Wind Tunnel for testing at higher transition speeds. The test section of the wind tunnel is oval in cross section with a length of 80 ft. The model was tested over a speed range of 40–100 kt. During the summer of 1989, the lower transition speed characteristics of the E-7A model were investigated in the rectangular 80 by 120-ft test section, which has an overall length of 120 ft. The larger test section dimensions permitted testing at airspeeds as low as 20 kt before significant flow recirculation effects were observed.

Baseline Aerodynamic Performance

The propulsion-induced effects on the E-7A airframe are by definition referenced to measurements of the aerodynamic performance of the model when the ejector diffusers, end plates, and upper ejector doors are stowed, and when the model is fitted with the 6-deg ventral nozzle. This is referred to as the sealed delta configuration and represents the up-and-away, cruise configuration of the model (Fig. 4).

In order to minimize propulsion system effects, the performance of the model in this configuration should be measured with either a flow-through engine inlet or with the engine inlet blocked off. It is, however, not possible to operate the full-scale model with the jet engine off due to inadequate lubrication when the engine is windmilling at low rpm. Predicting the spillage drag of the engine inlet in this configuration is also difficult.

Wind-on aerodynamic data were obtained with the engine operating at idle. From measurements of the ventral and rear nozzle static thrust, it was possible to subtract the small contributions to lift, drag, and pitching moment due to residual ventral and rear nozzle thrusts, and inlet ram drag at idle in order to obtain quasi-power-off aerodynamic performance. This method requires the assumption that the propulsion-induced effects due to interaction of the 6-deg ventral nozzle jet with the fuselage are negligible at low thrust levels. The power-off or thrust-removed aerodynamic coefficients for the sealed-delta configuration are shown in Eq. (1):

$$C_{L.A} = \frac{1}{qS}[L - T_{vn}\sin(\delta_{vn} + \alpha) - T_{rn}\sin\alpha]$$

$$C_{D.A} = \frac{1}{qS}[D - T_{vn}\cos(\delta_{vn} + \alpha) - T_{rn}\cos\alpha - D_{in}]$$

$$C_{m.A} = \frac{1}{qSc}\begin{bmatrix} M - T_{vn}\sin(\delta_{vn} + \alpha)d_{vn} \\ -T_{rn}\sin\alpha d_{rn/} - D_{in}d_{in} \end{bmatrix} \quad (1)$$

Figure 5 presents the thrust removed aerodynamic coefficients for the E-7A cruise configuration uncorrected for wind-tunnel wall effects. Data from the full-scale tests in the 80- by 120-ft wind tunnel are presented with comparison data from two scale-model tests. The $\frac{1}{9}$-scale model was configured with a cambered, wing, no tip missiles or launchers, and a flow-through inlet (moment reference center at 30% m.a.c.). It was tested at the General Dynamics Low Speed Tunnel (GDLST) in San Diego.[10] The 0.15-scale model was configured with a zero camber, zero twist wing (moment reference center at 31.4% m.a.c.). Engine inlet and exhaust flows were simulated using an ejector system within the fuselage.[4]

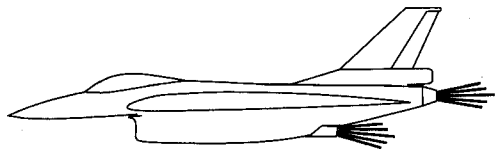

Fig. 4 E-7A Cruise configuration.

The lift curve measured at full-scale has approximately the same slope as the scale-model data, but is shifted down by nearly a constant increment. Calculations of the aerodynamic coefficients of the E-7A cruise configuration using the low-order panel method, PMARC,[13] predict a $\Delta C_L = -0.02$ at $\alpha = 0$ deg, due to the 6-deg washout in the wing of the full-scale model. This twist effect partially accounts for the lower lift observed at full scale. The full-scale drag polar closely matches the $\frac{1}{9}$-scale results, especially in the low C_L range. The 0.15-scale results show a lower drag from a C_L range of 0–0.75. Pitching moment coefficients from the full-scale model are larger than the results from the small-scale tests. The $C_{L.A} = 0$ intercept difference is about $\Delta C_m \approx 0.02$ at $C_L = 0$. The twist in the wing of the full-scale model partially accounts for the difference from the small-scale models which have wings with zero twist. The ΔC_m due to the washout is estimated to be +0.0038 at $\alpha = 0$ from the panel method calculation. The C_m of the unpowered, clean configuration at zero angle of attack is 0.0082 based on the PMARC calculation. The value measured during the full-scale tests is 0.0088. The differences in the locations of the moment reference centers for each of the models shift the C_m/C_L slopes about $C_{L.A} = 0$ by +0.04 ($\frac{1}{9}$-scale model) and by +0.026 (0.15-scale model) toward the value of ~0.02 evident in the full-scale data.

Propulsion-Induced Interference Effects

Ventral Nozzle Effects

The unique arrangement of the internal duct and valving system in the full-scale model made it possible to turn off the high-pressure air supply to the ejector system, and instead route it to the rear nozzle of the model. When operating in this configuration during wind-on testing, it was possible to make measurements of the propulsion-induced effects with only the ventral nozzle providing vertical lift. This configuration is shown schematically in Fig. 6, where the ventral nozzle thrust angle is vertical. Although this is not a realistic flight configuration, it provides the opportunity for comparison of ventral nozzle interference effects measured at small- and full-scale. Because of the extreme aft location and horizontal thrust line of the rear nozzle, it was assumed that the jet-induced effects on the airframe were negligible. A potential flow calculation of the effect of large model support strut fairings located beneath the model in the 80- by 120-ft wind tunnel (Fig. 1) showed a maximum ΔC_L of 0.02 due to support strut interference.[14] This effect was found to be localized in an area on the lower surface of the wing where the model is attached to the support system.

The ventral and rear nozzle static thrust and calculated engine inlet ram drag effects based on engine mass flow parameters are subtracted from the overall lift, drag, and pitching moments measured wind-on to obtain the power-effects-removed increment. The resulting aerodynamic coefficients are calculated in the same manner as Eq. (1). The ventral

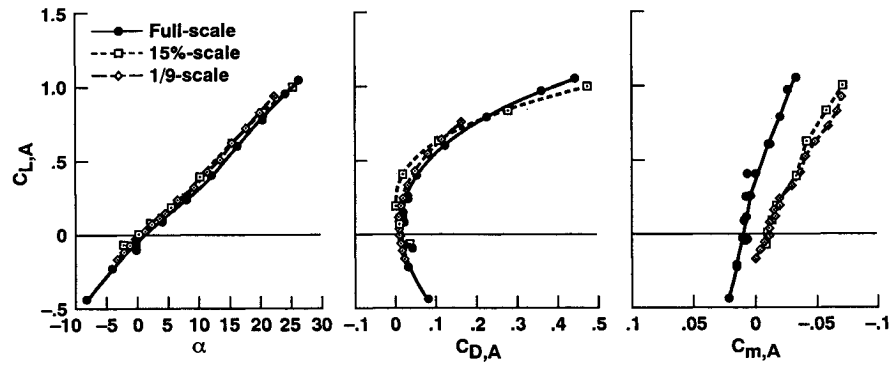

Fig. 5 Thrust-removed aerodynamic coefficients—cruise configuration, V_{ts} = 100 kt.

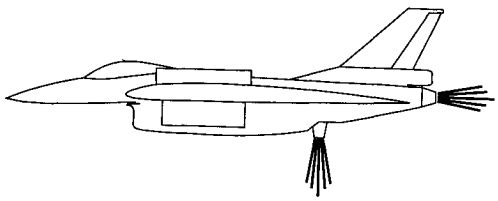

Fig. 6 Isolated ventral nozzle configuration.

nozzle induced effects are presented nondimensionalized by jet thrust. These effects are calculated as follows:

$$\frac{\Delta L}{T_{vn}} = \frac{[C_{L,A} - C_{L,A}(\text{baseline})]qS}{T_{vn}}$$

$$\frac{\Delta D}{T_{vn}} = \frac{[C_{D,A} - C_{D,A}(\text{baseline})]qS}{T_{vn}}$$

$$\frac{\Delta M}{T_{vn}c} = \frac{[C_{m,A} - C_{m,A}(\text{baseline})]qS}{T_{vn}} \quad (2)$$

The baseline power-effects-removed coefficients are obtained from low power runs in the sealed delta configuration.

During testing with the full-scale model in which only the ventral nozzle provided vertical lift, the ejector system inlet doors were open and the diffusers were fully deployed (Fig. 6). Large increments in drag as well as significant nose-down pitching moments are generated by these structures. The effects of ejector deployment drag can be added to the baseline coefficients by calculating a separate increment:

$$\frac{\Delta D}{T_{vn}} = \frac{[C_{D,A} - C_{D,A}(\text{baseline}) + \Delta C_{D,A}(\text{ejector})]qS}{T_{vn}} \quad (3)$$

The aerodynamic characteristics of the vehicle with the ejector deployed were measured using the full-scale model. This was accomplished by calculating the power-effects-removed coefficients of the model when it was configured with the ejectors off, but deployed, and with the ventral nozzle operating at engine-idle thrust levels. The induced effects on vehicle drag are then calculated as follows:

$$\frac{\Delta D}{T_{vn}} = \frac{[C_{D,A} - C_{D,A}(\text{ej-off.vn-off})]qS}{T_{vn}} \quad (4)$$

The propulsion-induced effects on vehicle pitching moments are calculated in a similar manner. Although none of the force and moment data used in the calculations are corrected for wind-tunnel wall effects, the propulsion-induced interference trends and magnitudes (when nondimensionalized by static thrust) are considered indicative of actual vehicle performance.

Figure 7 presents the interference effects due to the 90-deg ventral nozzle jet measured at full scale at α = 0, together

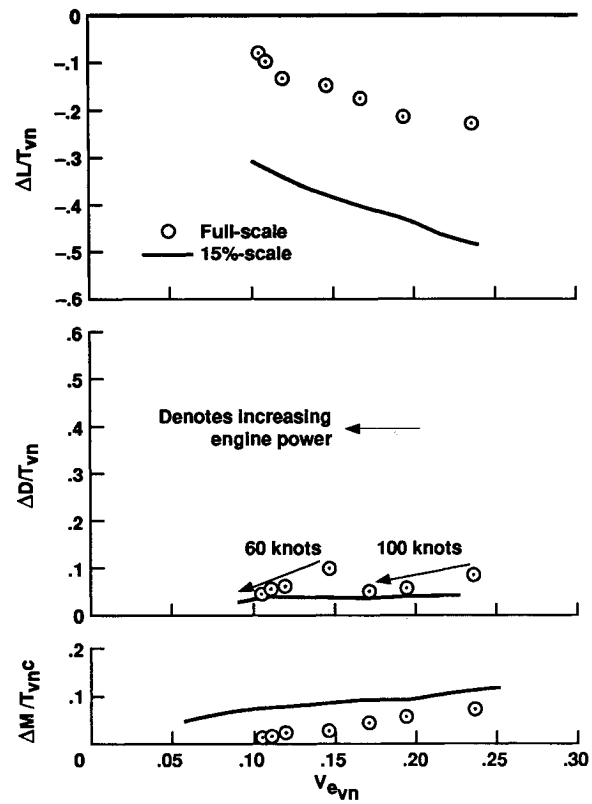

Fig. 7 Ventral nozzle induced effects, α = 0, δ_{vn} = 90 deg.

with results from tests of the 0.15-scale model. The induced effects are plotted vs effective velocity, which is defined as the ratio of freestream to jet velocities[15]

$$V_{evn} = \sqrt{\frac{q_\infty}{q_{jvn}}} \quad (5)$$

or using ventral nozzle static thrust

$$V_{evn} = \sqrt{\frac{q_\infty}{T_{vn}/2A_{vn}}} \quad (6)$$

The lift losses calculated from the full-scale data are much less than the small-scale results. One reason for the large discrepancies between the small- and full-scale results is the geometric differences between the ventral nozzles of the two models. The internal mechanization of the nozzle in the small-scale, free-flight model resulted in a highly skewed velocity profile at the exit of the nozzle compared with the relatively uniform velocity distribution of the full-scale nozzle. It is likely that the persistence of the potential core regions of the jets from the two models is substantially different due to the dif-

ferences in exit flow uniformity, although for neither test were the decay characteristics of the jets measured. The length of the jet core can have significant effects on the entrainment characteristics of jets.[5] It has also been shown that the characteristics of a lifting jet can significantly affect the interaction effects with an airframe.[16] The differences in lift loss may also be partially due to the greater relative vertical distance from the vertical nozzle exit plane to the lower surface of the wing at full-scale ($z_{vn} = 2.4d_{vn}$) than at small-scale ($z_{vn} = 1.8d_{vn}$). This is, however, only a weak effect.

The propulsion-induced drag effects calculated from the full- and small-scale data show good agreement. The induced drag effects at both small- and large-scale for isolated operation of the ventral nozzle are less than 10% of the nozzle thrust within the range of effective velocities tested. The lowest four and highest three full-scale data points on each plot represent clusters of data obtained at two tunnel speeds, while varying engine power. There is some interaction effect of the engine inlet flow with the airframe which results in an apparent increase in interference drag as engine power is increased at a given forward speed.

The full-scale induced effects show a greater nose-up pitching moment than the results from the small-scale model. This is an interesting result considering the reduced lift loss due to the ventral nozzle evident in the full-scale data. Since the ventral nozzle flowfield affects primarily the rear of the wing, a reduced ventral nozzle effect on lift should result in a reduced nose-up pitching moment.

Ejector System Effects

The ejector/augmentor system in the E-7A concept causes significant aerodynamic effects on both the lower and the upper surface of the vehicle. This is in contrast to the jet flow from the lifting ventral nozzle which affects primarily the lower surface of the wing and fuselage. During operation of the ejector system, a large quantity of ambient air is entrained into the ejector inlets on the upper surface of the wing. This is due to the mixing of the primary nozzle flow with the entrained ambient air which occurs within the ejector diffusers. The ratio of secondary or ambient airflow to primary or engine-supplied flow for the full-scale E-7A ejector system is approximately 9:1. The secondary airflow undergoes a rapid acceleration near the ejector inlets, and induces large negative pressures on the surrounding inlet and upper wing surfaces of the aircraft. These pressures have large effects on the vehicle lift and pitching moment.

The entrainment of freestream air into the relatively large, but low-velocity, ejector jets beneath the forward portion of the vehicle alters the upwash flowfield in which the wing is immersed. The angle of attack of the wing is reduced and a corresponding loss of wing lift occurs due to the presence of the lifting jets. In addition, a relatively large area of the lower fuselage surface is located between the diffuser exits of the twin longitudinal ejector systems. The pressure distribution on this area is dominated by the ejector exit flow conditions.

Propulsion-induced effects due to ejector operation on lift, drag, and pitching moment are calculated in a similar fashion to the ventral nozzle effects. An additional term is required in the equations for drag and pitching moment to account for the ejector inlet ram drag component. The moment arm used for calculation of the pitching moment increment due to d_{ejinl} was estimated to be $0.75D_H$, where D_H is the hydraulic diameter of the throat of a single ejector duct.[17] The equations for the power-effects removed aerodynamic coefficients are shown below:

$$C_{L,A_{ej}} = \frac{1}{qS}[L - T_{vn}\sin(\delta_{vn} + \alpha) - T_{ej}\cos\alpha]$$

$$C_{D,A_{ej}} = \frac{1}{qS}\left[D - T_{vn}\cos(\delta_{vn} + \alpha) - T_{ej}\sin\alpha - D_{in} - D_{ram}\right]$$

$$C_{m,A_{ej}} = \frac{1}{qSc}\left[M - T_{vn}\sin(\delta_{vn} + \alpha)d_{vn_h} - T_{ej}\cos\alpha d_{rn_h} - D_{in}d_{in} - D_{ram}d_{ejinl}\right] \quad (7)$$

In order to isolate the effects of the ejector system from the ventral nozzle which could not be turned off, the ventral nozzle deflection angle was set at 6 deg from the horizontal. A side view of this configuration is shown in Fig. 8.

In this configuration there are small interference effects due to interaction of the ventral nozzle jet with the lower portion of the fuselage aft of the nozzle exit. The small ventral nozzle induced effects were calculated from data obtained with the full-scale model in the cruise configuration. The residual ventral interference effects at an equivalent engine power setting are removed from the lift, drag, and pitching moment ejector effects as separate terms [see Eq. (8)]. One assumption of this technique is that the ejector and ventral nozzle interference effects are independent for low deflection angles of the ventral nozzle, e.g., $\delta_{vn} = 6$ deg. Additionally, this technique is only valid for conditions where $T_{ej} \cong T_{vn}$. With the nearly equal 48/52% thrust split between the ejectors and ventral nozzle, the maximum error introduced by this method is approximately $0.007\Delta L/T_{ej}$. The ejector system induced effects are calculated as follows:

$$\frac{\Delta L}{T_{ej}} = \frac{[C_{L,A_{ej}} - C_{L,A}(\text{baseline})]qS}{T_{ej}} - \frac{\Delta L}{T_{vn}}$$

$$\frac{\Delta D}{T_{ej}} = \frac{[C_{D,A_{ej}} - C_{D,A}(\text{baseline})]qS}{T_{ej}} - \frac{\Delta D}{T_{vn}}$$

$$\frac{\Delta M}{T_{ej}c} = \frac{[C_{m,A_{ej}} - C_{m,A}(\text{baseline})]qS}{T_{ej}} - \frac{\Delta M}{T_{vn}c} \quad (8)$$

The propulsion-induced effects, due to ejector system operation, will be presented as a function of the effective velocity of the vehicle in the ejector configuration. This velocity ratio parameter is expressed as

$$V_{e_{ej}} = \sqrt{\frac{q_\infty}{q_{j_{ej}}}} \quad (9)$$

or using ejector static thrust

$$V_{e_{ej}} = \sqrt{\frac{q_\infty}{T_{ej}/2A_{ej}}} \quad (10)$$

Figure 9 presents the lift, drag, and pitching moment interference effects due to isolated operation of the ejector system calculated from the full-scale test data, as well as effects measured with a 0.15-scale model. Within the range of effective velocities tested at full-scale, there is very good agreement between the 0.15-scale and large-scale lift and drag induced effects. The full-scale results show a slightly higher lift loss than the small-scale trend at higher values of V_e. The effects of ejector system operation on vehicle lift are approximately twice as large as the ventral-induced effects at an equivalent effective velocity. In both the small- and large-scale results, a lift loss of up to 40% of ejector thrust occurs at values of $V_e > 0.4$. These results were calculated from data obtained at a model angle of attack of

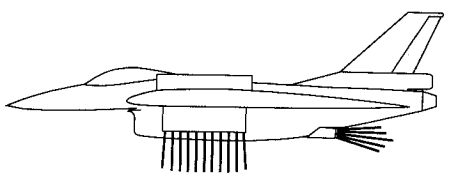

Fig. 8 Isolated ejector configuration.

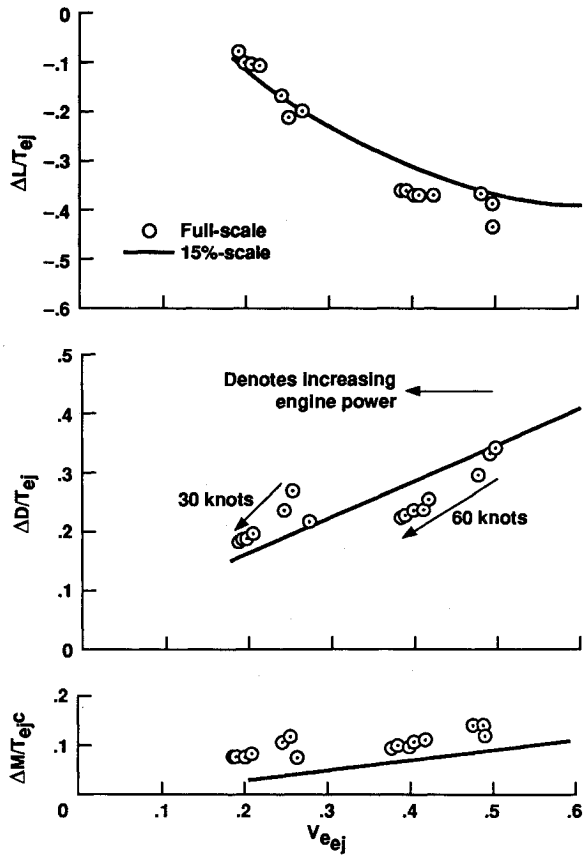

Fig. 9 Ejector system induced effects, $\alpha = 0$, $\delta_{vn} = 6$ deg.

0 deg. During transition to wingborne flight, STOVL aircraft will assume a progressively greater nose-up pitch attitude in order to transfer from powered lift at low airspeeds to wingborne flight. Above a V_e of about 0.3 (50–60 kt), the induced lift loss can be recovered by pitching the vehicle up to an angle of attack of 8 deg, or by an elevon deflection of 20 deg.

Several factors account for the substantial positive increment in induced effects on vehicle drag observed in both the small- and large-scale results. At forward airspeed, the secondary air which flows into the ejector inlets on the upper surface of the wings must be turned through an angle of 90 deg in order to flow downward through the ejector ducts. The momentum drag created by reducing the streamwise component of freestream velocity of the ejector secondary air to zero appears as pressure forces on the rearward and forward facing surfaces of the ejector inlet lips. The pressures on the rearward facing inlet lip located at the front of the ejector are less than the pressures on the rear surface. This results in a net increase in drag and nose-up pitching moment. In addition, the bluff body aerodynamic drag of the ejector diffusers located beneath the wings contributes a counteracting nose-down pitching moment increment. Each of these drag effects is included in the overall force measurements which are used to calculate the drag increments.

Because the jet engine was operating in the full-scale model, the effect of the momentum or ram drag due to the jet engine inlet has been removed from the full-scale data. In contrast, the ejector-driven, ventral nozzle simulator in the small-scale model was turned off for this configuration. Freestream flow was permitted to pass through the engine inlet duct and exit from the ventral nozzle. It was assumed that no ram drag was produced by the flow. There was probably a small drag increment generated by the friction of the flow as it passed through the duct. This is not accounted for in the small-scale data.

The pitching moment interference effects calculated from the full-scale data show a greater nose-up moment. This is due to greater secondary flow entrainment of the ejector system in the full-scale model. The thrust augmentation ratio for the ejectors in the 0.15-scale model is approximately 1.4.[3] For the full-scale model the augmentation ratio is approximately 1.58.[12] Secondary flow entrainment is directly proportional to the thrust augmentation ratio. The nose-up pitching moment is generated by the momentum transfer effects of turning the ejector secondary flow at a chordwise location ahead of the moment reference center.

Combined Operation of Ejector System and Ventral Nozzle

The E-7A model is capable of producing representative lifting jets when both the ejector system and ventral nozzle are operated simultaneously. Induced effects in this configuration, shown in Fig. 10, were evaluated at forward speed using the full-scale model. Although the turbulence levels and temperatures within the jets are similar to future, ejector-configured STOVL concepts, the Spey powerplant in the E-7A model does not fully simulate the pressure ratios and resultant thrust levels required for an actual flight vehicle. The ventral nozzle pressure ratio produced by the Spey powerplant, ~1.8, is also considerably less than the value of 3.0 which could be delivered by a F-110 engine. The exit area of the ventral nozzle is also smaller for the Spey-powered model than for a F-110-powered vehicle.

The induced effects on vehicle aerodynamics due to combined operation of the ejector system and ventral nozzle are expressed as a fraction of the total propulsion system thrust. The lift, drag, and pitching moment increments are calculated as follows:

$$\frac{\Delta L}{T_{tot}} = \frac{[C_{L,A_{tot}} - C_{L,A}(\text{baseline})]qS}{(T_{ej} + T_{vn})}$$

$$\frac{\Delta D}{T_{tot}} = \frac{[C_{D,A_{tot}} - C_{D,A}(\text{baseline})]qS}{(T_{ej} + T_{vn})}$$

$$\frac{\Delta M}{T_{tot}c} = \frac{[C_{m,A_{tot}} - C_{m,A}(\text{baseline})]qS}{(T_{ej} + T_{vn})} \tag{11}$$

where

$$C_{L,A_{tot}} = \frac{1}{qS}[L - T_{vn}\sin(\delta_{vn} + \alpha) - T_{ej}\cos\alpha]$$

$$C_{D,A_{tot}} = \frac{1}{qS}\begin{bmatrix} D - T_{vn}\cos(\delta_{vn} + \alpha) - T_{ej}\sin\alpha \\ -D_{in} - D_{ram} \end{bmatrix}$$

$$C_{m,A_{tot}} = \frac{1}{qSc}\begin{bmatrix} M - T_{vn}\sin(\delta_{vn} + \alpha)d_{vn_h} \\ -T_{ej}\cos\alpha d_{rn_h} - D_{in}d_{in} \\ -D_{ram}d_{ejinl} \end{bmatrix} \tag{12}$$

The total propulsion system induced effects are presented as a function of a weighted effective velocity. Although there is greater than an order of magnitude difference in the exit velocities of the ejector and ventral nozzle jets, the contributions to propulsive lift from each jet are nearly equal. The effective velocities calculated from ejector and ventral nozzle thrusts are weighted by the fraction of total propulsion system thrust provided by each of the elements. The ejector and ventral nozzle contributions are then summed. The weighted effective velocities were tested at full-scale over a range of $0.1 < V_{e_w} < 0.6$. This weighted V_{e_w} is calculated as follows:

$$V_{e_w} = \frac{T_{ej}}{(T_{ej} + T_{vn})}\sqrt{\frac{q_\infty}{T_{ej}/2A_{ej}}} + \frac{T_{vn}}{(T_{ej} + T_{vn})}\sqrt{\frac{q_\infty}{T_{vn}/2A_{vn}}} \tag{13}$$

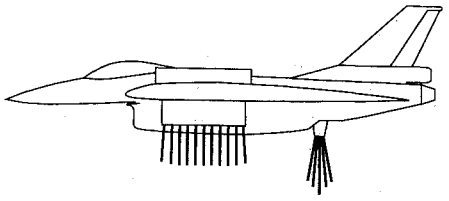

Fig. 10 E-7A Hover configuration.

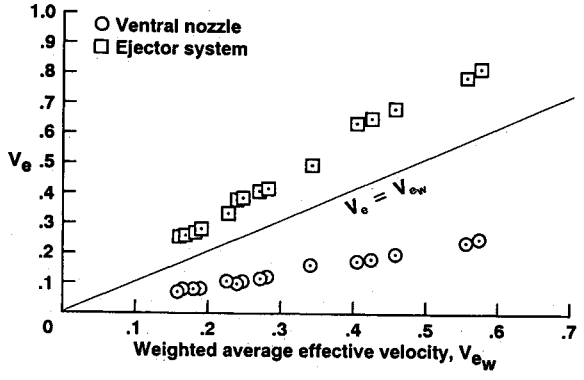

Fig. 11 Relationship of effective jet velocities.

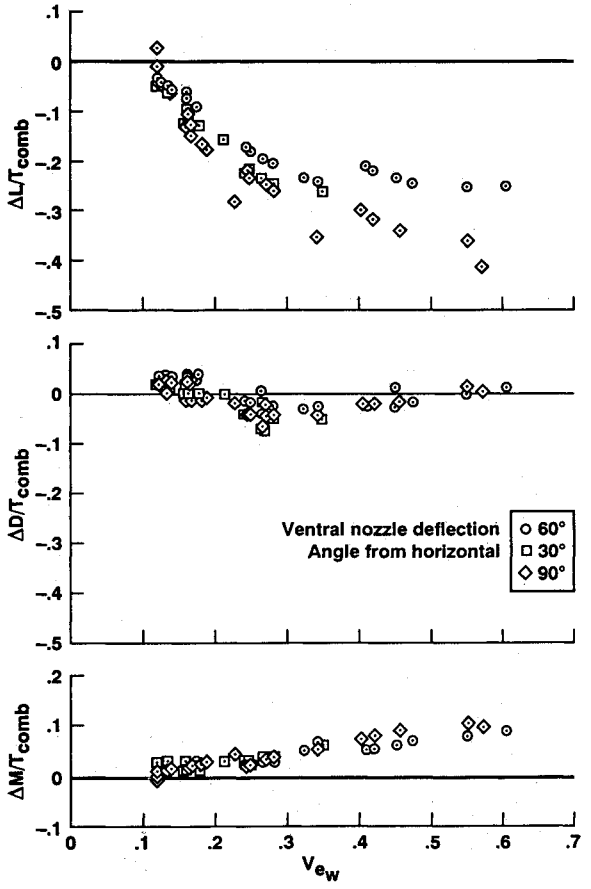

Fig. 12 Induced effects for combined operation of ejector system and ventral nozzle, $\alpha = 0$.

Figure 11 presents a comparison of the effective velocities for isolated ventral nozzle and ejector system operation plotted vs the weighted effective velocity based on the individual components. The data were obtained at a wide variety of engine power settings and tunnel velocities in the 80- by 120-ft wind tunnel. It can be seen that for a given weighted effective velocity, the V_e in ejector mode is more than three times greater than the ventral nozzle value. Actual jet velocities are inversely proportional to the effective velocities. The diagonal line on the plot illustrates the locus of points for $V_e = V_{ew}$.

Figure 12 presents the induced effects on lift, drag, and pitching moment calculated from the full-scale data. These data were obtained over a tunnel speed range of $20 < V_\infty < 100$ kt in the test section of the 80- by 120-ft wind tunnel. The variation of the magnitude of these effects due to change of the thrust vector angle of the ventral nozzle is shown in the figure. It can be seen that the induced lift losses for combined operation of the ejectors and ventral nozzle is approximately the same order of magnitude as the isolated ejector interference effects, especially at high thrust deflection angles of the ventral nozzle. Lift losses with the 90-deg ventral nozzle are larger than either the 60- or 30-deg configurations above a V_e of approximately 0.2. In a realistic STOVL transition sequence, the thrust vector angle of the ventral nozzle will decrease from 90 deg in order to maintan adequate vehicle acceleration.

The induced effects on the drag of the model are slightly positive at both the lowest and highest range of effective velocities tested. Only over the range of $0.2 < V_e < 0.45$ (~60 kt at full thrust) is a negative trend apparent. The negative drag evident within this V_e range is an unexpected result. The combined effects of forward velocity, jet entrainment, and interaction of the ejector flow with the ventral nozzle jet produce a small net negative drag on the model at certain jet velocity ratios. The data indicate that at a V_e of 0.25, there is a net forward thrust on the vehicle which is equal to approximately 5% of propulsion system thrust (~500 lbf). This is quite surprising, considering that the induced effects on drag due to isolated operation of the ejector system are positive and amount to nearly 20% of ejector thrust at an equivalent effective velocity. Uncertainties in measurement of drag in the 80- by 120-ft wind tunnel are approximately ±41 lb. Uncertainties in the procedure for removing the direct thrust increments from the propulsive/lift jets are estimated to be equal to ±112 lb. Summing these uncertainties results in an equivalent uncertainty in $\Delta D/T_{comb}$ of approximately 0.015 (approximately the size of the data symbols).

There is some experimental evidence that the induced effects due to simultaneous operation of multiple lifting jets in certain configurations are less than the sum of the contributions of the individual jets. Small-scale test results for combined operation of the ejector system and a 60-deg ventral nozzle show that the measured values of induced lift, drag, and pitching moment are smaller in magnitude than would be obtained by summing the contributions of the individual elements.[18] Measurements of the pressures in the ejector throat of the full-scale E-7A data show a more negative pressure at the aft end of the ejectors with increasing thrust vector angle of the ventral nozzle in forward flight.[19] This pressure shift can result in an apparent vectoring of the ejector exit flow toward the rear of the vehicle.

The pitching moment effects are similar in magnitude to the isolated ventral nozzle effects. Both the drag and pitching moment trends appear to be only a weak function of the thrust vector angle of the ventral nozzle.

Concluding Remarks

A full-scale wind-tunnel model of an ejector-lift/vectored-thrust STOVL fighter aircraft has been used to measure propulsion-induced aerodynamic effects in terms of lift, drag, and pitching moment increments. Aerodynamic effects of isolated operation of the lifting ejector system and vectorable ventral nozzle are presented as well as those effects which arise from simultaneous operation of all lifting jets. The full-scale results from isolated operation of the forward and aft lifting systems generally follow the trends of earlier small-scale tests. When all lifting jets are operated at the same time, lift and pitching moment trends are similar to the isolated jet cases. Jet in-

teraction effects cause a small negative drag or thrust on the airframe when the lifting ejectors and ventral nozzle are operated simultaneously at certain forward speeds. It has been demonstrated that full-scale tests of a powered STOVL model can be used to obtain propulsion-induced effects on an ejector-configured, supersonic fighter concept with multiple lifting jets.

References

[1]Margason, R. J., "Propulsion-Induced Effects Caused by Out-of-Ground Effects," *Proceedings of the International Powered Lift Conference*, Society of Automotive Engineers, Dec. 1987, pp. 31–57.

[2]Banks, D. W., and Gatlin, G. M., "Longitudinal and Lateral Aerodynamic Data from Tests of an Advanced STOVL Fighter Employing a Powered Lift Ejector," NASA TM-87672, May 1986.

[3]Riley, D. R., Shah, G. H., and Kuhn, D. E., "Some Power-Induced Effects for Transition Flight Measured on a 0.15-Scale E-7A STOVL Fighter Model," NASA TM-4188, June 1990.

[4]Riley, D. R., Shah, G. H., and Kuhn, D. E., "Low-Speed Wind-Tunnel Results of a 0.15-Percent-Scale Model of an E-7A STOVL Fighter Configuration," NASA TM-4107, July 1989.

[5]Lye, J. D., and Jewitt, C., "Data Report on a New Ejector Lift/Vectored Thrust V/STOL Model in the NAE 30 × 30-Foot Low Speed Wind Tunnel," Dept. of National Defence, WT-FA-1, DHC-DND 86-1, Ottawa, Canada, March 1986.

[6]Poppen, W. A., "Determination of Ejector-Induced Aerodynamic Interference Forces and Moments Using Data from the 0.3-Scale E-7A Model," General Dynamics Fort Worth Division Rept., Aeroanalysis Internal Memorandum 638, Oct. 1987.

[7]Henderson, J. F., "E-7A Aero Data Documentation," General Dynamics Fort Worth Division Rept., Aerodynamic Stability and Control Technical Memorandum 89-017, Aug. 1988.

[8]Benepe, D. B., "Effect of Scale on V/STOL Operation in Ground Proximity for a Turbojet Engine," NASA CR-177504, Sept. 1988.

[9]Foley, W. H., Sheridan, A. E., and Smith, C. W., "Study of Aerodynamic Technology for Single-Cruise-Engine V/STOL Fighter Attack Aircraft: Phase I Final Report," NASA CR-166268, Feb. 1982.

[10]Foley, W. H., Albright, A. E., and Smith, C. W., "Study of Aerodynamic Technology for Single-Cruise-Engine V/STOL Fighter Attack Aircraft: Phase II Final Report," NASA CR-177367, Aug. 1985.

[11]Lye, J. D., "Report on Wind Tunnel Tests of the Full-Scale E-7A Model with a Rolls Royce Spey 801 SF Engine in the NASA Ames 40 × 80 Foot Tunnel," Dept. of National Defence, DHC-DRIE 89-02, Ottawa, Canada, 1989.

[12]Poppen, W. A., "Test and Analysis Report on the Full-Scale E-7A Model in the NASA Ames 40 × 80 Foot Tunnel with Emphasis on the Aero-Propulsion Induced Effects in Transition," General Dynamics ERR-FW-4006, May 1990.

[13]Ashby, D. L., Dudley, M. R., Iguchi, S. K., Browne, L., and Katz, J., "Potential Flow Theory and Operation Guide for the Panel Code PMARC," NASA TM-102851, Jan. 1991.

[14]Ashby, D. L., and Harris, S. H., "Use of a Potential Flow Code for Wind-Tunnel Wall Corrections," NASA TM 104019, Oct. 1993.

[15]Margason, R. J., "Jet V/STOL Wind Tunnel Simulation and Groundplane Effects," Paper 15, AGARD CP-308, Oct. 1981.

[16]Gentry, G. L., and Margason, R. J., "Jet-Induced Lift Losses on VTOL Configurations Hovering In and Out of Ground Effect," NASA TN D-31666, Feb. 1966.

[17]Henderson, C., Clark, J., and Walters, M., "V/STOL Aerodynamics and Stability & Control Manual," Naval Air Development Center 80017-60, Jan. 1980.

[18]Vogler, R. D., "Interference Effects of Single and Multiple Round or Slotted Jets on a VTOL Model in Transition," NASA TN D-2380, Aug. 1964.

[19]Smith, B. E., Garland, D., and Poppen, W. R., "Aerodynamic Performance of a Lifting Ejector System in a STOVL Fighter Aircraft," AIAA Paper 92-3094, July 1992.